The International Archives of the Photogrammetry, Remote Sensing and Spatial Information Sciences, Volume XLVIII-G-2025
ISPRS Geospatial Week 2025 “Photogrammetry & Remote Sensing for a Better Tomorrow…”, 6–11 April 2025, Dubai, UAE

Single camera 6-dof object tracking using spatial resection based techniques

Milad Davoudkhani, Christian Mulsow, Hans-Gerd Maas

Institute of Photogrammetry and Remote Sensing, TUD Dresden University of Technology, Germany
(milad.davoudkhani, christian.mulsow, hans-gerd.maas)@tu-dresden.de

Keywords: object tracking, spatial resection, single high-speed camera, close range photogrammetry.

Abstract

Photogrammetric methods and advanced algorithms are widely used for tracking objects in camera image sequences in various sectors, such as motion analysis, industrial inspection, monitoring of environmental processes, or analyzing impact events or explosions. The use of multi camera stereo photogrammetry systems is a common approach to track objects in 3D. Nevertheless, single camera based solutions may be particularly valuable in scenarios where only one camera can be used due to constraints such as cost limitations, synchronization requirements, or spatial observation conditions. This will especially be the case, if powerful high-speed cameras are being employed.
This paper presents a photogrammetric approach based on spatial resection principles for using a single camera for 3D object tracking. The method utilizes direct computation of velocity and acceleration as well as rotation parameters of a moving object in 3D space, allowing for the determination of the object’s position and trajectory from image sequences captured by a single high-speed camera. The method is derived from the inverse spatial resection, where a stationary camera observes a moving object of known geometry and the apparent changes of the six camera exterior orientation parameters obtained from spatial resection are transferred into 6-dof object motion parameters. In our developed spatial resection based object tracking method, 12 unknown parameters are calculated. Different from conventional spatial resection, these 12 parameters are the first and second derivatives of the 6 exterior orientation parameters (three linear translations plus three angular orientation elements) over time. The approach is implemented in a way that these 12 motion parameters can be determined directly from an arbitrary number of images (at least three) of an image sequence, thus significantly enhancing precision and reliability.
The method has undergone rigorous testing and validation using both simulated data as well as real data obtained in a civil engineering impact monitoring experiment observed by a high-speed camera. In addition to explaining the methodology, the paper presents the results of these validation tests.

1. Introduction

Photogrammetry offers powerful options in 3D object tracking, both of single or multiple objects. Beyond 3D trajectory data, photogrammetric techniques also allow for the determination of 6-dof (degrees of freedom) information, thus describing translation and rotation of objects simultaneously.
Object tracking has gained recent interest across a variety of sectors, including civil engineering, environmental medicine, and industrial applications. One application of object tracking is, for instance, in robot calibration using photogrammetry and single or stereo camera solutions to verify that the robot arm is positioned in relation to its nominal location (Maas, 1997). Object tracking was also used in three dimensional velocity and trajectory measurement of moving particles in fluid (3D PTV) and its utilization in complex flow measurement applications (Maas et al., 1993). Another application of object tracking can be found in space collisions. Space debris impacts are expected to increase in the future, and the created fragments after these impacts may pose a serious problem. Because of that, it is critical to have accurate orbital debris models based on space debris observed from Earth to assess the risk of satellites operating in any particular orbit (Liou, 2006).
The development of methods for tracking objects can help to improve the accuracy of these models. With this motivation, several methods and algorithms in photogrammetry and computer vision have been developed for object tracking using camera systems and image processing, such as tracking of fragmentation and calculation of objects data as velocity and size using a single high-speed video camera and algorithms for data analysis in hypervelocity impact experiments (Watson et al., 2019). In civil engineering, object tracking plays an essential role, for example, in some important analyses in improvement of the resistance of construction materials. The Research Training Group GRK 2250 of the German Research Foundation is developing suitable measurement and evaluation techniques for analyzing the performance of different mineral-bonded composites and validating numerical simulations with the goal of enhancing the impact resistance of existing buildings by applying thin layers of strengthening material (Mechtcherine and Curosu, 2017). 3D object tracking is one of the important techniques in analysis that contributes to achieving this goal.
There are very different solutions for navigation and tracking of an object: inertial navigation systems (INS), GPS/INU for in-situ airborne camera orientation, laser triangulation with multiple transmitters, laser tracking, photogrammetric stereo and multi-image point tracking, and photogrammetric single camera object tracking (Luhmann, 2009). In choosing the right method for object tracking in a project, various factors such as size and speed of the object to be tracked play a very important role.
In photogrammetric techniques, the appropriate choice of imaging devices according to the required spatio-temporal resolution and duration of an event is essential. Stereo based 3D reconstruction techniques, applied to multi-camera image sequences, allow for the determination of 3D translation and rotation parameters of rigid objects. However, in various fields, the use of a single camera may be appealing for measuring position, trajectory, velocity, acceleration, and rotation parameters of a moving object

in 3D. For applications where the use of multiple cameras is not well feasible, often due to cost restrictions, lack of precise synchronization, or specific observation space conditions, single-camera solutions may depict an appealing alternative. Single camera based 6-dof object tracking may be realized by the principle of inverse spatial resection (Luhmann, 2009), where a stationary camera observes a moving object of known geometry and the apparent changes of the six camera exterior orientation parameters obtained from spatial resection are transferred into 6-dof object motion parameters.
One of the applications of using a single camera for object tracking is in monitoring the wheel motion of a car in all six degrees of freedom using a single high speed camera. It calculates non-contactly the orientation and spatial position of a moving wheel with respect to the stable reference system of the car body (Wiora et al., 2004). Another example is in tracking systems where a handheld probe is observed by a single camera as an optical tracking system, and the determination of 6-dof is performed in real time (Luhmann, 2023).
The paper focuses on 6-dof object tracking by using a photogrammetric method based on spatial resection in single high speed cameras image sequences. Our goal is to formulate the inverse spatial resection based 6-dof tracking approach in a way that the motion parameters can be determined directly from image observations, and to extend the technique to the direct determination of 3D translation and rotation parameters plus their first and second derivatives in time. Moreover, the approach is designed in a way that it can be applied to an arbitrary number of images of an image sequence, rather than to single images, and that the underlying motion model may be adapted to various types of motion.

2. Methodology

In this study, we utilize the photogrammetric resection method, integrated with physics equations of motion, to determine the required parameters for analyzing object movement.

2.1 Spatial resection

Spatial resection in photogrammetry is the process of determining the six exterior orientation parameters of the camera based on photographic measurements of object points whose XYZ ground coordinates are known. The six exterior orientation parameters are the coordinates of the exposure station (X_0, Y_0, Z_0) and the angular orientation elements (ω, Φ, κ) in a 3x3 rotation matrix r_{ij}. The minimum requirement for spatial resection with a calibrated camera is three (non-collinear) points, but most solutions take more points and come with least-squares solutions.

$$x_p = x_0 + c\frac{r_{11}(X - X_0) + r_{21}(Y - Y_0) + r_{31}(Z - Z_0)}{r_{13}(X - X_0) + r_{23}(Y - Y_0) + r_{33}(Z - Z_0)} + \Delta\acute{x} \tag{1}$$

$$y_p = y_0 + c\frac{r_{12}(X - X_0) + r_{22}(Y - Y_0) + r_{32}(Z - Z_0)}{r_{13}(X - X_0) + r_{23}(Y - Y_0) + r_{33}(Z - Z_0)} + \Delta\acute{y} \tag{2}$$

Where x_p and y_p are the image coordinate of point p and x_0, y_0 are coordinates of the principal point and c is the camera focal length, X and Y and Z represent object coordinates of point p, $\Delta\acute{x}$ and $\Delta\acute{y}$ are correction terms (distortion) and r_{ij} are elements of the rotation matrix $R_{\omega\phi\kappa}$ (3×3).

2.2 Motion types

In the domain of object tracking, it is essential to comprehend the principles of motion and the governing equations. There are various types of motion that an object can exhibit, such as linear motion, parabolic motion, circular motion, or wave motion. In the paper, we concentrate on the two models linear and parabolic motion that occur in object tracking applications in civil engineering impact experiments. Linear motion occurs when an object moves in a straight line with a constant velocity. In parabolic motion the object follows a curved path in the shape of a parabola. Parabolic motion can be defined as a form of movement that comprises both accelerated and uniform components, such as the motion of object affected by gravity. An object that moves with constant velocity of v in a direction for a duration of t will have a displacement of s in that same direction:

$$s = v \cdot t \tag{3}$$

The displacement s and velocity v of an object moving with constant acceleration a and initial velocity v_0 are connected by the following equations after time t.

$$s = v_0 \cdot t + \frac{1}{2} \cdot a \cdot t^2 \tag{4}$$

$$v = v_0 + a \cdot t \tag{5}$$

2.3 Method description

Our photogrammetric method utilizes spatial resection for 6-dof object tracking. When an image captures a moving object, we assume that the object is in actual motion while the camera remains fixed. Our object tracking method inversely assumes a stationary object and a camera moving from frame to frame (Figure 1). When dealing with multiple objects, it is assumed that each object is associated with its own camera (virtual camera), and the analysis for object tracking can be performed independently for each object.

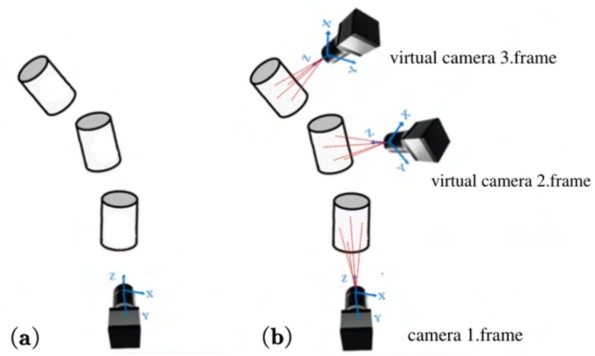

Figure 1. (a) A single camera capturing a moving object. (b) Illustration of the method for tracking object motion

Through the analysis of each virtual camera movement, we can infer the motion of objects. In the conventional approach (which will be replaced by a direct computation of velocity and acceleration here later on), the camera's external orientation parameters are calculated for each frame based on a set of 3D point coordinates on the object that is assumed to be rigid. The disparities among these computed parameters are employed to ascertain the distance traversed by the object between frames. The object's velocity can be calculated by dividing the distance traveled by the time between frames, and acceleration by dividing the velocity difference by time. The Helmert transformation is used to calculate the transformed object coordinates of each point in the next frames with calculated parameters by spatial resections.

$$X = T + R \cdot X' \tag{6}$$

$$\begin{bmatrix} X \\ Y \\ Z \end{bmatrix} = \begin{bmatrix} t_x \\ t_y \\ t_z \end{bmatrix} + \begin{bmatrix} r_{11} & r_{12} & r_{13} \\ r_{21} & r_{22} & r_{23} \\ r_{31} & r_{32} & r_{33} \end{bmatrix} \cdot \begin{bmatrix} X' \\ Y' \\ Z' \end{bmatrix} \tag{7}$$

where X' is the initial vector, X is the transformed vector, R is the rotation matrix and T is translation vector.
In our approach, instead of directly calculating the external orientation parameters of the camera for each frame, we implemented the spatial resection with 6 unknowns directly describing uniform motion, as seen in Eq. 8, and increased the number of unknowns from 6 to 12 for accelerated motion, represented in Eq. 9. The unknowns to be determined from the image coordinate measurements are first and second derivatives of the external orientation parameters of the camera over time. The first derivatives provide us with the velocity, while the second derivatives give us the acceleration of the moving camera. Furthermore, our spatial resection based approach may be applied to all images in an image sequence or to any subset of images with constant time intervals to track the object, rather than between every two frames only, thus significantly increasing redundancy and thus precision and determinability of parameters.

$$u = \begin{bmatrix} \frac{\delta X}{\delta t} \\ \frac{\delta Y}{\delta t} \\ \frac{\delta Z}{\delta t} \\ \frac{\delta \omega}{\delta t} \\ \frac{\delta \phi}{\delta t} \\ \frac{\delta \kappa}{\delta t} \end{bmatrix} = \begin{bmatrix} v_{X_i} \\ v_{Y_i} \\ v_{Z_i} \\ v_{\omega_i} \\ v_{\phi_i} \\ v_{\kappa_i} \end{bmatrix} \tag{8}$$

$$u = \begin{bmatrix} \frac{\delta X}{\delta t} \\ \frac{\delta Y}{\delta t} \\ \frac{\delta Z}{\delta t} \\ \frac{\delta \omega}{\delta t} \\ \frac{\delta \phi}{\delta t} \\ \frac{\delta \kappa}{\delta t} \\ \frac{\delta^2 X}{\delta t^2} \\ \frac{\delta^2 Y}{\delta t^2} \\ \frac{\delta^2 Z}{\delta t^2} \\ \frac{\delta^2 \omega}{\delta t^2} \\ \frac{\delta^2 \phi}{\delta t^2} \\ \frac{\delta^2 \kappa}{\delta t^2} \end{bmatrix} = \begin{bmatrix} v_{X_i} \\ v_{Y_i} \\ v_{Z_i} \\ v_{\omega_i} \\ v_{\phi_i} \\ v_{\kappa_i} \\ a_{X_i} \\ a_{Y_i} \\ a_{Z_i} \\ a_{\omega_i} \\ a_{\phi_i} \\ a_{\kappa_i} \end{bmatrix} \tag{9}$$

In uniform motion, the equations are as follows:

$$\begin{cases} T_i = T_0 + \dfrac{\partial T}{\partial t} \cdot \Delta t \\ R_i = R_0 + \dfrac{\partial R}{\partial t} \cdot \Delta t \end{cases} \tag{10}$$

T_0 are the initial translation parameters at time t_0 and $\frac{\partial T}{\partial t}$ represent the rate of change of the translation parameters, i.e., velocity (first derivative); and R_0 are initial rotation parameters at time t_0 and $\frac{\partial R}{\partial t}$ the rate of change of rotation parameters, i.e., rotational velocity (first derivative).
In accelerated motion, the equations are as follows:

$$\begin{cases} T_i = T_0 + \dfrac{\partial T}{\partial t} \cdot \Delta t + \dfrac{1}{2} \cdot \dfrac{\partial^2 T}{\partial t^2} \cdot \Delta t^2 \\ R_i = R_0 + \dfrac{\partial R}{\partial t} \cdot \Delta t + \dfrac{1}{2} \cdot \dfrac{\partial^2 R}{\partial t^2} \cdot \Delta t^2 \end{cases} \tag{11}$$

where T_0 and R_0 are initial translations and rotation parameters at time t_0, $\frac{\partial T}{\partial t}$ and $\frac{\partial R}{\partial t}$ represent the velocity, $\frac{\partial^2 R}{\partial t^2}$ and $\frac{\partial^2 T}{\partial t^2}$ are the rate of change of velocity of translation and rotation parameters, i.e. acceleration (second derivative).
Also the external orientation parameters of the camera in the i-th image can be computed using the following equations:

$$X_i = X_0 + \frac{\partial X}{\partial t} \cdot (i \cdot \Delta t) + \frac{1}{2} \cdot \frac{\partial^2 X}{\partial t^2} \cdot (i \cdot \Delta t)^2 \tag{12}$$

$$Y_i = Y_0 + \frac{\partial Y}{\partial t} \cdot (i \cdot \Delta t) + \frac{1}{2} \cdot \frac{\partial^2 Y}{\partial t^2} \cdot (i \cdot \Delta t)^2 \tag{13}$$

$$Z_i = Z_0 + \frac{\partial Z}{\partial t} \cdot (i \cdot \Delta t) + \frac{1}{2} \cdot \frac{\partial^2 Z}{\partial t^2} \cdot (i \cdot \Delta t)^2 \tag{14}$$

$$\omega_i = \omega_0 + \frac{\partial \omega}{\partial t} \cdot (i \cdot \Delta t) + \frac{1}{2} \cdot \frac{\partial^2 \omega}{\partial t^2} \cdot (i \cdot \Delta t)^2 \tag{15}$$

$$\phi_i = \phi_0 + \frac{\partial \phi}{\partial t} \cdot (i \cdot \Delta t) + \frac{1}{2} \cdot \frac{\partial^2 \phi}{\partial t^2} \cdot (i \cdot \Delta t)^2 \tag{16}$$

$$\kappa_i = \kappa_0 + \frac{\partial \kappa}{\partial t} \cdot (i \cdot \Delta t) + \frac{1}{2} \cdot \frac{\partial^2 \kappa}{\partial t^2} \cdot (i \cdot \Delta t)^2 \tag{17}$$

3. Method evaluation with simulated data

In this section, we describe a first evaluation of our method using simulated data. Simulated data provides a controlled environment where specific scenarios and parameters can be precisely adjusted, enabling a detailed analysis of the method's performance and robustness. Obviously, the validation with simulated data should be accompanied by real experiments, which will be shown in section 4. To evaluate the performance of our method, we generated coordinates of 3D points on a cylindrical object and projected these with the model based on collinearity equations with given internal and external orientations parameters to calculate the image coordinates of generated object points in a sequence of simulated images. The simulation data includes various motion scenarios that cover potential variations in real-world data. In the initial scenario, the object undergoes translational and rotational motion in the X, Y, and Z directions in 10 steps. Each step corresponds to a time interval of 1 second. This is a uniform linear motion with constant velocity. The results of motion parameter determination by our model as outlined in section 2 as well as the standard deviations of the 6 linear motion parameters are shown in Table 1 and Figures 2 and 3.

Parameter	Value	Standard deviation
vx (mm/s)	2.800	3.598e-17
vy (mm/s)	1.100	1.927e-17
vz (mm/s)	1.500	5.291e-17
vω (rad/s)	0.00698	1.905e-18
vϕ (rad/s)	0.00523	1.551e-18
vκ (rad/s)	0.00174	1.305e-18

Table 1. The results of parameter determination.

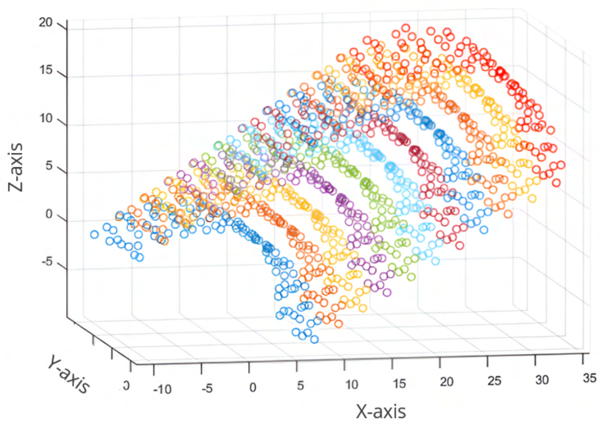

Figure 2. Visualization of the object's motion across 11 frames.

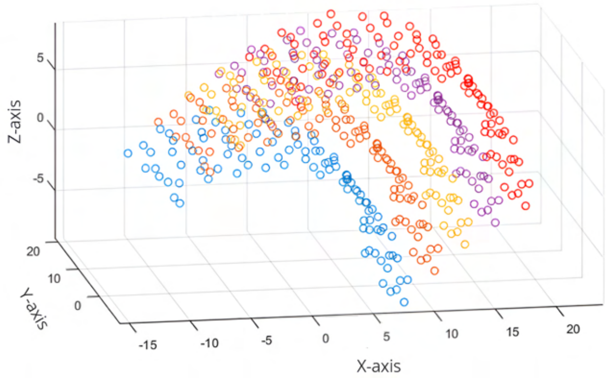

Figure 4. Visualization of the object's movement across 5 frames.

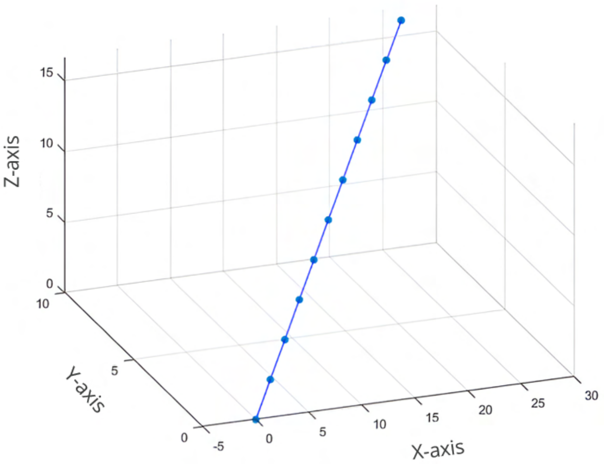

Figure 3. Trajectory of the object across 11 frames.

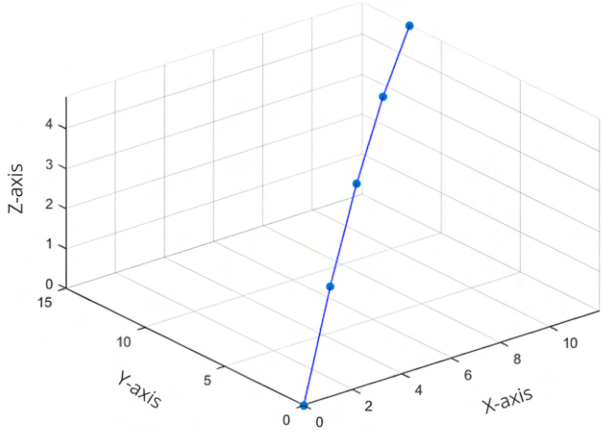

Figure 5. Trajectory of the object over 5 frames.

In a second scenario, the object moves parabolically. The object's motion is uniform in the x and y directions, moving in a straight line at a constant velocity with each step being 3 millimeters, and in the z direction, the motion is accelerated in 4 steps, with each step corresponding to a 1-second time interval. The results are displayed in Table 2 and Figures 4 and 5.

Parameter	Value	Standard deviation
vx (mm/s)	3.000	3.576e-08
vy (mm/s)	3.000	1.313e-08
vz (mm/s)	2.000	1.309e-08
$v\omega$ (rad/s)	6.780e-11	4.519e-11
$v\phi$ (rad/s)	2.979e-11	4.363e-11
$v\kappa$ (rad/s)	1.067e-11	1.953e-11
ax (mm/s²)	-1.124e-08	2.075e-08
ay (mm/s²)	2.649e-08	2.224e-08
az (mm/s²)	-0.400	7.575e-09
$a\omega$ (rad/s²)	-3.069e-11	2.627e-11
$a\phi$ (rad/s²)	-1.323e-11	2.532e-11
$a\kappa$ (rad/s²)	5.300e-12	1.136e-11

Table 2. The results of parameter determination.

Obviously, the results are almost perfect. However, this only validates the correctness of the implementation of the model, as perfect simulated data without any measurement noise were used.

3.1 Simulation parameter variations

This section presents results obtained by modifying the parameters in the simulation.

3.1.1 Impact of image measurement errors on parameter estimates: In order to evaluate the efficacy of the method and assess the influence of errors in image coordinates on the results of the method, the object was shifted by 0.1 mm in the X, Y, and Z directions and rotated by 0.1 degrees around all three axes over five frames, with a time difference of one second between each frame. Then the image coordinates have been corrupted by random noise of 1 micrometer (0.05 pixel). The simulation was performed with a camera constant of 105 mm and a recording distance of 80 cm. The corrupted image coordinates were then used to solve for the 12 unknown parameters of the method. This process was repeated 1000 times. The differences between the computed parameters using data with errors and the calculated parameters using noise-free data were computed each time and then averaged. The results are presented in Figures 6 and 7, as well as Table 3.

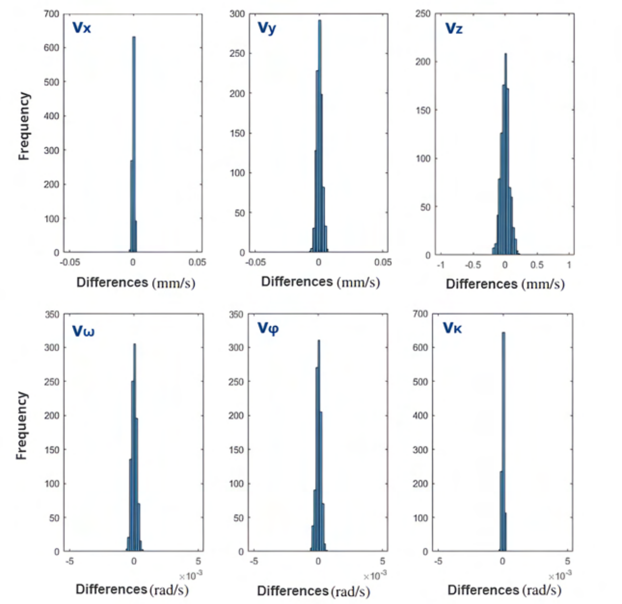

Figure 6. Frequency distribution of differences between 6 calculated velocity parameters values with random errors and the error-free data, based on 1000 trials.

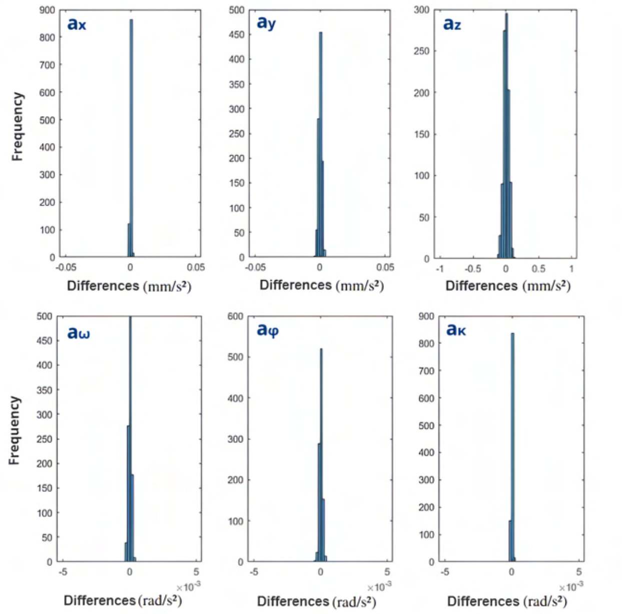

Figure 7. Frequency distribution of differences between 6 calculated acceleration parameters with random errors and error-free data from 1000 trials.

Parameter	Mean Value	Parameter	Mean Value
vx (mm/s)	-2.387e-05	ax (mm/s²)	1.115e-05
vy (mm/s)	8.076e-05	ay (mm/s²)	-4.868e-05
vz (mm/s)	-0.002	az (mm/s²)	0.001
vω (rad/s)	3.733e-06	aω (rad/s²)	1.594e-06
vϕ (rad/s)	-5.507e-06	aϕ (rad/s²)	1.289e-06
vκ (rad/s)	1.610e-06	aκ (rad/s²)	1.005e-06

Table 3. The mean of the discrepancies between the calculated parameters from data with randomly error and error-free data.

The results show that the averages of differences for two of the parameters, v_z and a_z, are significantly larger than those for the other 10 parameters. This indicates that these two parameters are more sensitive to image coordinate measurement errors.

3.1.2 Object size: The influence of the object size on the standard deviation of each parameter of the method was tested with changing the object size, and the object in simulated data was scaled by factors of 0.5, 0.7, 2, and 5. It is expected that the inverse spatial resection based technique delivers the best results if the tracked object fills the complete image format, while a smaller object size (or a larger distance) leads to a deterioration of the precision of parameter determination. The results presented in Table 4 demonstrate the extent to which the standard deviations enhance as the size of the object increases. In conclusion, larger objects provide better accuracy, as expected. This result is also in accordance with results of research on suitable lengths in reference bar calibration strategies (Maas, 1999).

Scale factor	Standard deviation
0.7 - 1	25.61%
1 - 2	49.31%
0.5 - 2	71.62%
0.5 - 5	84.27%

Table 4. Effect on the standard deviation of 12 parameters.

3.1.3 Focal length: Modifying the focal length as a parameter of the interior orientation is also done to evaluate the method and impact of variations on the results. The analysis can demonstrate the extent to which changing lenses from wide to small angles affects the standard deviation of the method's calculated parameter. A change in the focal length at constant image size affects the results. The standard deviation of all of the 12 parameters of spatial resection is affected by variation of the focal length. The standard deviations of 12 parameters improve by 61.20% when the focal length is increased from 25 mm to 125 mm. As a conclusion, the longer focal length or narrower angle of view improves the accuracy of results.

4. Method evaluation with real data and experiments

Following the successful evaluation with simulation data, we proceeded to test our method with real data obtained from actual experiments. This section outlines the application of the method to real-world data and presents the results of this evaluation. An experiment was conducted in the lab to validate our method in real-world scenarios. A cylindrical concrete specimen with a 40 mm length and 22 mm diameter was chosen as the object for the experiment, and for accurate measurements, a stochastic pattern was applied to the object surface (Figure 8). As the imaging device, a single high-speed camera, the Photron Fastcam SA X2 at full resolution (1024×1024 px at 12500 fps), was used. The main technological specifications of this camera are listed in Table 5. A 1kW-LED-4438 lighting system with 100,000 lm in continuous operation was used. Figure 9 shows the experimental setup.

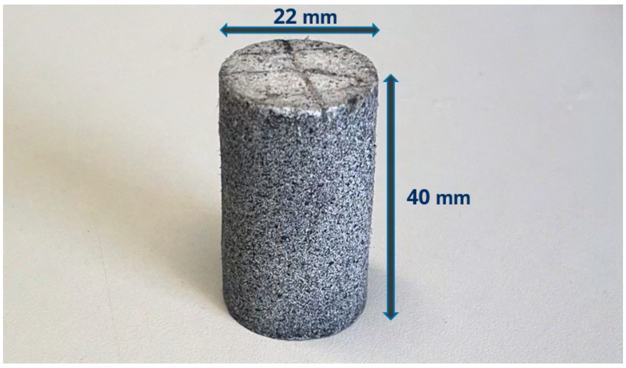

Figure 8. Cylindrical concrete specimen

Sensor type	CMOS,Monochrome model
Pixel Size	20 µm × 20 µm
Sensor Size	20.48 × 20.48 mm
Maximum Resolution	1024 × 1024 px at 12500 fps
Maximum Frame Rate	480,000fps for 128 × 48 px
Fill Factor	58%
Minimum Exposure	Global electronic shutter to 1µs

Table 5. Main specifications of the Photron Fastcam SA-X2 high-speed camera (Photron, 2017).

Figure 9. Experimental setup (Photron camera and two lamps in the foreground, holder and specimen in the background)

An initial crucial step involved calibrating the high-speed camera. A self calibration approach (Luhmann et al., 2015) was employed to determine the camera parameters of the experimental setup. An image block consisting of 36 images of a test field was captured in a camera calibration scheme as suggested in (Godding, 1993). The resulting standard deviation of the unit weight is σ_0 = 0.95 µm (0.048 pixel) and the average standard deviation of object point coordinates obtained from bundle block adjustment was RMSX = 5 µm RMSZ = 4 µm and RMSY = 7 µm. Note that the coordinate system was oriented with the Z-axis in the camera viewing direction. The calibration parameters were used to rectify and remove effects of distortions and displacements in all captured images for 3D model reconstruction and motion analysis. The distortion model by Brown (Brown, 1971) was used for rectification of images.

The experiment was conducted using a holder with six markers attached to it and placed in 79 cm from the camera. At first, the object was hung from above using a string to keep it still while creating a 3D model of the object using a standard structure from motion method and capturing the first frame. 3D object coordinates of 241 points were determined by 3D model reconstruction by capturing overlapping images from different views. The next steps involved the calculation of pixel coordinates of object points in the first frame of motion recording and the calculation of the camera pose of this frame. Subsequently, the object was released, allowing it to rotate while falling in order to achieve both translational and rotational motion for tracking purposes. This motion was captured using a single high-speed camera. 800 frames were recorded for analysing the object motion and the recording duration was 64 ms (time difference between frames = 80 µs).

After the calculation of 3D object coordinates and their image coordinates in the first frame of motion image sequences (Figure 10), least squares matching (LSM) was used to track each image point in the first frame in sequences consisting of 800 frames. LSM matches the corresponding points across images with sub-pixel accuracy by minimizing the sum of the squares of gray value differences between the patches of pixels in two consecutive images (Gruen, 1985). After matching, the pixel coordinates were converted to metric image coordinates.

$$x = -\frac{s_x}{2} + u \cdot p_x \tag{18}$$

$$y = \frac{s_y}{2} - v \cdot p_y \tag{19}$$

where s_x and s_y represent the size of the sensor and px, py are pixel size and the variables u and v are pixel coordinates.

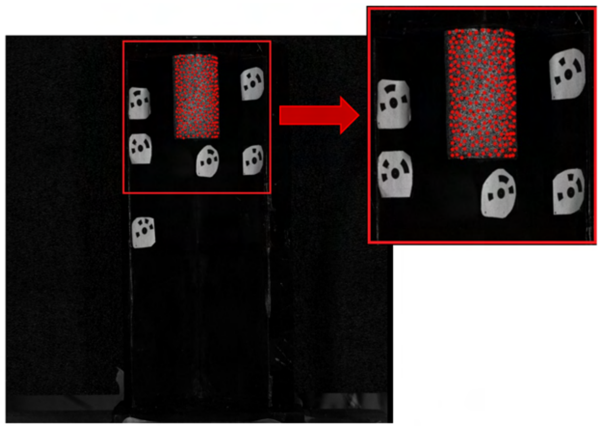

Figure 10. Projected 3D object coordinates in first frame of motion image sequences

The elapsed time of each frame was computed, and all image coordinates were then saved in a file along with their corresponding time values. The image coordinates file consisted of 192800 image coordinate pairs (241 points in 800 frames). Our photogrammetric method based on spatial resection for tracking was used with all 800 images simultaneously rather than 800 times between two consecutive images each. That means that the 12 parameters of accelerated motion were directly determined from the image sequence, promising much better precision and noise behavior. The results are shown in Figures 11, 12, and Table 6.

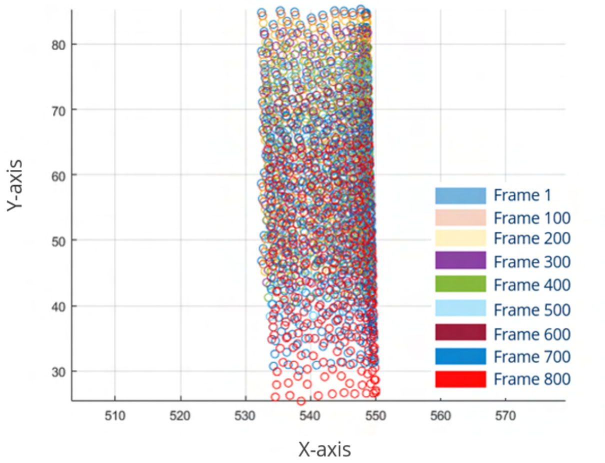

Figure 11. Visualization of the object's movement over each 100th frame.

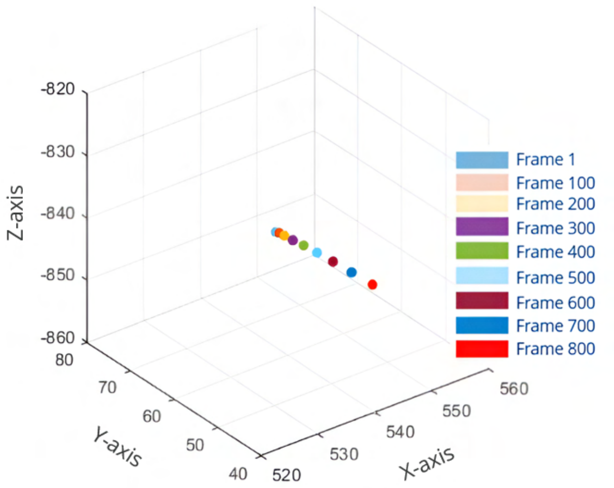

Figure 12. Trajectory of the object over each 100th frame.

Note that the coordinate system was oriented with the Z-axis in the camera viewing direction and the motion is in the Y direction.

Parameter	Value	Standard deviation
vx (mm/s)	22.095	0.182
vy (mm/s)	20.066	0.035
vz (mm/s)	21.938	0.359
$v\omega$ (rad/s)	0.227	0.002
$v\phi$ (rad/s)	0.091	0.003
$v\kappa$ (rad/s)	0.448	0.001
ax (mm/s²)	37.750	7.251
ay (mm/s²)	9776.909	1.358
az (mm/s²)	249.387	14.310
$a\omega$ (rad/s²)	3.469	0.114
$a\phi$ (rad/s²)	1.184	0.125
$a\kappa$ (rad/s²)	1.893	0.066

Table 6. The calculated 12 unknown parameters and their standard deviation in spatial resection.

The position-time graph of X, Y, and Z and the angular position-time graph of omega, phi, and kappa are shown in figures 13 and 14.

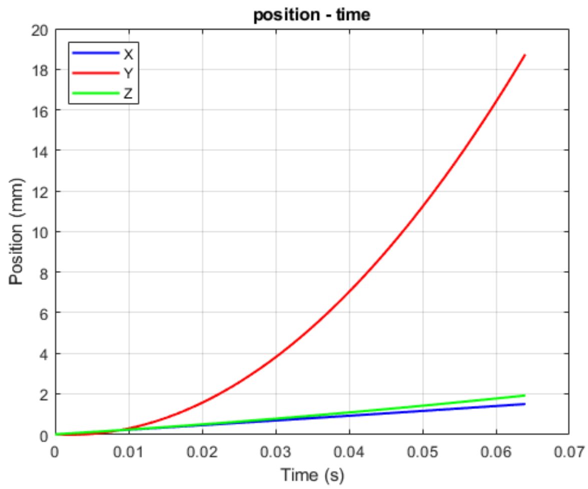

Figure 13. The position-time graph of translation parameters.

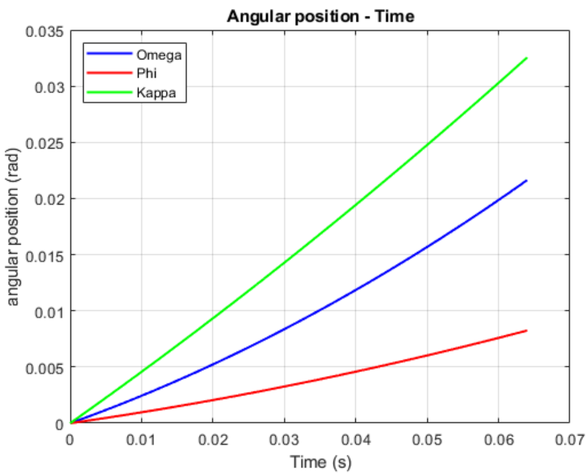

Figure 14. The angular position-time graph of rotation parameters.

The acceleration in the Y-direction is clearly dominant, reaching almost gravity acceleration. The velocity is not zero, as image acquisition intentionally started shortly after the release of the specimen. The results show that the velocity accuracy in the Y direction is higher than in the X and Z directions, as errors are limited to the distance measurement due to the absence of time errors. Moreover, the longer the distance measured, the greater the accuracy. The rotational acceleration in omega is larger than the other two, which can also be seen in the curved blue graphs in Figure 14; this indicates a gravity-induced tilting of the specimen.
In the next step, the standard deviations of the parameters were determined using a reduced number of images, i.e., only introducing each 2nd, 4th, 8th, etc., image into the simultaneous inverse spatial resection. The calculated ratio was the same for each parameter. Table 7 shows the results of the comparison. The comparative analysis demonstrates how the standard deviations change when using subsets of the images compared to using all images. As expected, analysis reveals a trend where standard

deviations increase as fewer images are used.

Images	Standard deviation
800 (all images)	100%
400 (every 2nd image)	140%
200 (every 4th image)	198%
100 (every 8th image)	273%
50 (every 16th image)	365%

Table 7. Effect of the number of images on the standard deviation of parameters.

5. Conclusion

The paper presents a novel approach of single camera 3D 6-dof object tracking based on a modified inverse spatial resection approach, wherein 6, respectively 12 parameters describing linear or accelerated 3D motion are determined directly from an arbitrary number of images of an image sequence. A 3D object to be tracked is represented by a sufficient number of 3D points, which are, for instance, determined using the SfM approach. These points are then tracked through an image sequence with subpixel accuracy using least-squares matching. The results are fed into a modified inverse spatial resection applied to an arbitrary number of images of the image sequence, either introducing 6 or 12 parameters of linear or accelerated motion as unknowns. The results of experiments both with simulated and real data show a very good precision potential of the method. The parametrization may easily be altered and extended for other types of motion. The method is especially of interest for experiments with high-speed or ultrahigh-speed cameras, where stereo setups may be difficult to arrange due to the cost of the devices or due to spatial limitations. Future work will extend the approach from single to multiple object tracking, possibly by also introducing constraints between the motion parameters of neighboring objects.

References

Brown, D. C., 1971. Close-Range Camera Calibration. *Photogrammetric Eng.*, 37, 855-866.

Godding, R., 1993. Photogrammetric method for the investigation and calibration of high-resolution camera systems. L. Beiser, R. K. Lenz (eds), *Recording Systems: High-Resolution Cameras and Recording Devices and Laser Scanning and Recording Systems*, 1987, SPIE, 103 – 110. Backup Publisher: International Society for Optics and Photonics.

Gruen, A. W., 1985. Adaptive least squeres correlation: A powerful image matching technique. *South African Journal of Photogrammetry, Remote Sensing and Cartography*, Vol. 14, 175-187.

Liou, J.-C., 2006. Collision activities in the future orbital debris environment. *Advances in Space Research*, 38(9), 2102–2106.

Luhmann, T., 2009. Precision potential of photogrammetric 6DOF pose estimation with a single camera. *ISPRS Journal of Photogrammetry and Remote Sensing*, 64(3), 275–284.

Luhmann, T., 2023. *Nahbereichsphotogrammetrie*. Wichmann, Germany.

Luhmann, T., Fraser, C., Maas, H.-G., 2015. Sensor modelling and camera calibration for close-range photogrammetry. *ISPRS Journal of Photogrammetry and Remote Sensing*, 115.

Maas, H.-G., 1997. Dynamic photogrammetric calibration of industrial robots. *Proceedings of SPIE - The International Society for Optical Engineering*, 3174, 106–112.

Maas, H.-G., 1999. Image sequence based automatic multi-camera system calibration techniques. *ISPRS Journal of Photogrammetry and Remote Sensing*, 54(5-6), 352–359.

Maas, H. G., Gruen, A., Papantoniou, D., 1993. Particle tracking velocimetry in three-dimensional flows. *Experiments in Fluids*, 15(2), 133–146.

Mechtcherine, V., Curosu, I., 2017. Mineral-Bonded Composites for Enhanced Structural Impact Safety – A New Research Training Group GRK 2250 of the German Research Society. *Procedia Engineering*, 210, 182–185.

Photron, 2017. Photron Fastcam SA-X2 Datasheet (8 Juli 2024).

Watson, E., Kunert, N., Putzar, R., Maas, H.-G., Hiermaier, S., 2019. Four-View Split-Image Fragment Tracking in Hypervelocity Impact Experiments. *International Journal of Impact Engineering*, 135, 103405.

Wiora, G., Babrou, P., Männer, R., 2004. Real time high speed measurement of photogrammetric targets. C. E. Rasmussen, H. H. Bülthoff, B. Schölkopf, M. A. Giese (eds), *Pattern Recognition*, Springer Berlin Heidelberg, Berlin, Heidelberg, 562–569.